JOURNAL OF SOLID STATE CHEMISTRY **127,** 98–108 (1996)
ARTICLE NO. 0362

Investigation of Grinding Effects in Binary Mixtures from the TiO_2–SnO_2–V_2O_5 System

S. Begin-Colin,[1] G. Le Caër, A. Mocellin, C. Jurenka, and M. Zandona

Laboratoire de Sciences et Génie des Matériaux Métalliques, CNRS UA 159, Ecole des Mines, 54042 Nancy Cedex, France

Received March 4, 1996; in revised form July 22, 1996; accepted August 14, 1996

Solid solution formation induced by dry ball-milling under an argon atmosphere has been investigated in binary mixtures from the TiO_2–SnO_2–V_2O_5 system mainly by X-ray diffraction and differential scanning calorimetry. Grinding experiments followed by heat treatments result in substantial solid solubilities in all three binaries. Under our experimental conditions, the solubility after grinding depends solely on the nature of grinding media particularly in V_2O_5 based systems, when reduction reactions take place between grinding tools and oxide particles. The results demonstrate that the interaction between TiO_2 or SnO_2 and V_2O_5 follows from the fact that SnO_2 and TiO_2 are first slightly reduced during milling and subsequently reoxidized by V_2O_5. These interactions promote solid solution formation and the development of a reduced disordered vanadium oxide layer at the surface of SnO_2 grains. The final state of powders, where the interface density between both oxides is very high, could be of interest in catalysis.

INTRODUCTION

Mechanical alloying is an original and now widely used method to synthesize various materials, often metastable, with nanometer-sized grains (1, 2). A wide variety of compounds and alloys have been obtained by this dry and high energy ball milling process (3, 4), as well as high pressure and/or high temperature oxide phases and some nonequilibrium structures that cannot be obtained at room temperature (5, 6). In particular, immiscible binary metallic phase diagrams have been investigated and very large metastable solid solubilities have been attained. For instance, Polkin *et al.* (7) observed extended solid solubilities in several systems such as Al–Fe and Ni–W and Gaffet *et al.* (8, 9) and Faudot *et al.* (10) in the Cu–Fe and Cu–W systems. Similarly Sundaresan and Froes (11) report Mg solubilities up to 6 at.% in mechanically alloyed Ti–Mg alloys, whereas its equilibrium solubility is less than 0.2 at.%. Recently the solubility of tin in chromium has been extended from less than 1 at.% to 10 at.% (12, 13). Thus, the formation of extended metastable solid solutions by grinding has been well demonstrated in metallic systems (4), but has just begun to be investigated in oxide systems.

Recent articles report polymorphic transformations induced by milling upon single oxides (5, 14–18) or binary oxide systems such as ZrO_2–M_xO_y with M = Y, Ca, Fe, Mg, . . . (18–20).

In this paper the TiO_2–SnO_2, TiO_2–V_2O_5, and SnO_2–V_2O_5 systems have been investigated mainly because their miscibilities are not very well known and the previously reported influence of grinding on the single oxides TiO_2 and SnO_2 should moreover allow a better understanding of mechanisms (6). Moreover, V_2O_5-based binary oxide systems are of great interest in catalysis for selective oxidation of hydrocarbons or ammonidation processes (21–23) and maximum contact between both oxides leads to maximum activity. Mechanical alloying precisely provides a means to substantially increase the interface area.

—The binary phase diagram of TiO_2–SnO_2 exhibits a miscibility gap with a critical temperature close to 1430°C at ≈47 mol% TiO_2 (24–26). The solid solution between TiO_2 and SnO_2 has the rutile structure.

—The TiO_2–V_2O_5 and SnO_2–V_2O_5 systems have been widely studied in relation to their applications as catalysts. SnO_2 and TiO_2 are added as promoters of the catalytic activity of V_2O_5. These systems have been investigated with different methods of synthesis and in a general way, solid solutions form by introduction of V^{4+} ions in the lattice of TiO_2 or SnO_2 (22, 27–36). In many publications, the solid solubility of vanadium in tin oxide is still discussed. In the TiO_2–V_2O_5 system, the main observations point to the decrease of the phase transformation temperature of the anatase form into the rutile one (600°C instead of 850–1100°C) when anatase is in presence of V_2O_5 and also to the formation of solid solutions (up to 6.5 to 8 wt% of V_2O_5, that is up to 6.1 to 7.6 at.% of V^{4+} in $(Ti_{1-x}V_x)O_2$) (30–33,37–39).

High activity and selectivity of V_2O_5-based catalysts are achieved when vanadia is present in the form of highly disordered, amorphous or reduced species at the surface

[1] To whom correspondence should be addressed.

0022-4596/96 $18.00

of SnO_2 grains (18, 32–33, 37). In V_2O_5–MO_2 (M = Ti, Sn) catalysts, the latter properties are usually attributed to the presence of TiO_2 or SnO_2 although their precise explanations are still lacking. Many attempts are currently made to clarify the structure of this catalyst.

Although the study of mechanochemical reactions is not the main purpose of our paper, redox reactions play a role in the phenomena which occur by grinding binary mixtures from the TiO_2–SnO_2–V_2O_5 system. All kinds of mechanochemical reactions have been considered in detail in various papers (40–46) to which the readers are refered. The purpose of this work consists of investigating the formation of solid solutions induced by grinding in these binary oxide systems. Different techniques such as Mössbauer spectroscopy, X-ray diffraction, and differential thermal analysis were used. Previous studies of polymorphic transformations induced by milling in single oxides have demonstrated the influence of the nature of milling media in particular when oxido-reduction reactions take place between grinding tools and oxide particles (6). Thus, experiments were performed with grinding media of different natures (oxide or metallic).

EXPERIMENTAL PROCEDURE

The starting powder materials were anatase TiO_2 (Labosi, $\phi = 5\ \mu m$) or rutile (Cerac, $\phi = 10\ \mu m$) with tetragonal structures, Cassiterite SnO_2 (Labosi, $\phi = 5\ \mu m$, tetragonal structure), SnO (Aldrich, $\phi = 10\ \mu m$, tetragonal structure), and V_2O_5 (Aldrich, $\phi = 2\ \mu m$, orthorhombic structure). Continuous grinding, i.e., uninterrupted, was performed under an argon atmosphere in a planetary ball mill (Fritsch Pulverisette 7) either with a steel vial (50 cm^3) and steel balls (seven balls of diameter close to 13 mm) or with a vial (50 cm^3) and six balls (diameter close to 12 mm) of yttria-stabilized zirconia. Contamination by tools, although often neglected, may play an important role in the transformations which take place in many materials during grinding. To characterize the effect of contamination, we have used two sets of steel tools with different hardnesses. The steel grinding tools (Fe + 13%Cr) were either untreated or hardened by annealing and quenching treatments. The initial experiments were performed with untreated steel and proved that steel reacts in an important way with oxide powders. The Vicker's hardness of the latter steel has been increased by thermal treatments from 275 to 760. The powder to ball weight ratio (R) is generally 1/40 with steel tools and 1/10 with zirconia tools. The powders were introduced in the vial in equimolar proportions and sealed in a glove box under an argon atmosphere.

The specific shock power P released by the balls to the powders, which is the product of the shock frequency and the kinetic energy, during the ball-milling process has been calculated for our experimental conditions from the model of Abdellaoui and Gaffet (47, 48, and personal communication). They are:

—$P \approx 2.7$ W/g/ball for steel tools and $R = 1/40$;
—$P \approx 0.9$ W/g/ball for yttria-stabilized zirconia tools and $R = 1/10$.

The resulting products have been characterized by X-ray diffraction (XRD) using Co$K\alpha$ radiation. The different solid solubilities in the three binary oxide systems have been calculated from lattice constants of SnO_2 or TiO_2 according to Vegard's law. The fact that the variation of the cell volume is not due to grinding effects has been confirmed by grinding experiments on MO_2 oxides alone. In the case of the SnO_2–TiO_2 system, the SnO_2 lattice volume has been calculated with the (110), (101), (211), (002), (202), (321) diffraction peaks and in the SnO_2–V_2O_5 system with (220), (002), (202), (321), (222), (312), (411) diffraction peaks because of the overlapping of some SnO_2 and V_2O_5 diffraction peaks.

The powder mixtures containing SnO_2 were studied by ^{119}Sn Mössbauer spectroscopy at room temperature. The contamination by steel was followed by room temperature ^{57}Fe Mössbauer spectroscopy. As usual, the ^{119}Sn and ^{57}Fe isomer shifts are given with respect to $BaSnO_3$ and α-Fe at room temperature, respectively.

The thermal stabilities of the different phases were investigated with a SETARAM low (1073 K) temperature differential scanning calorimeter (DSC). The powders were heated up to 1073 K at a rate of 5 K/min and cooled down to room temperature at a rate of 10 K/min without steps. The observed exothermic or endothermic peaks on the DSC curves enable the detection of reactions or melting of compounds.

RESULTS AND DISCUSSION

(1) SnO_2

As described below, the understanding, based on ^{119}Sn Mössbauer spectrometry, of phenomena occurring in powder mixtures containing tin oxides plays a major role in the interpretation of the behavior of other systems too. We will therefore briefly present the results obtained by tin Mössbauer spectroscopy for ground SnO_2 powders. Figure 1a shows the usual spectrum of SnO_2 with a slightly broadened single line with $a \sim 0$ mm/s isomer shift. SnO_2 remains unaffected when ground with zirconia tools (6). When ground with untreated steel tools, SnO_2 is by contrast reduced to $SnO_{1.74\pm0.04}$ as shown by the characteristic doublet of Sn^{2+} with a quadrupole splitting of 1.92 mm/s (Fig. 1b) (6). When ground with hardened steel tools (Fig. 1c), a less marked reduction of SnO_2 to $SnO_{1.83\pm0.03}$ is observed. No reduction at all is even observed when new vials and balls are used. The incorporation of iron atoms

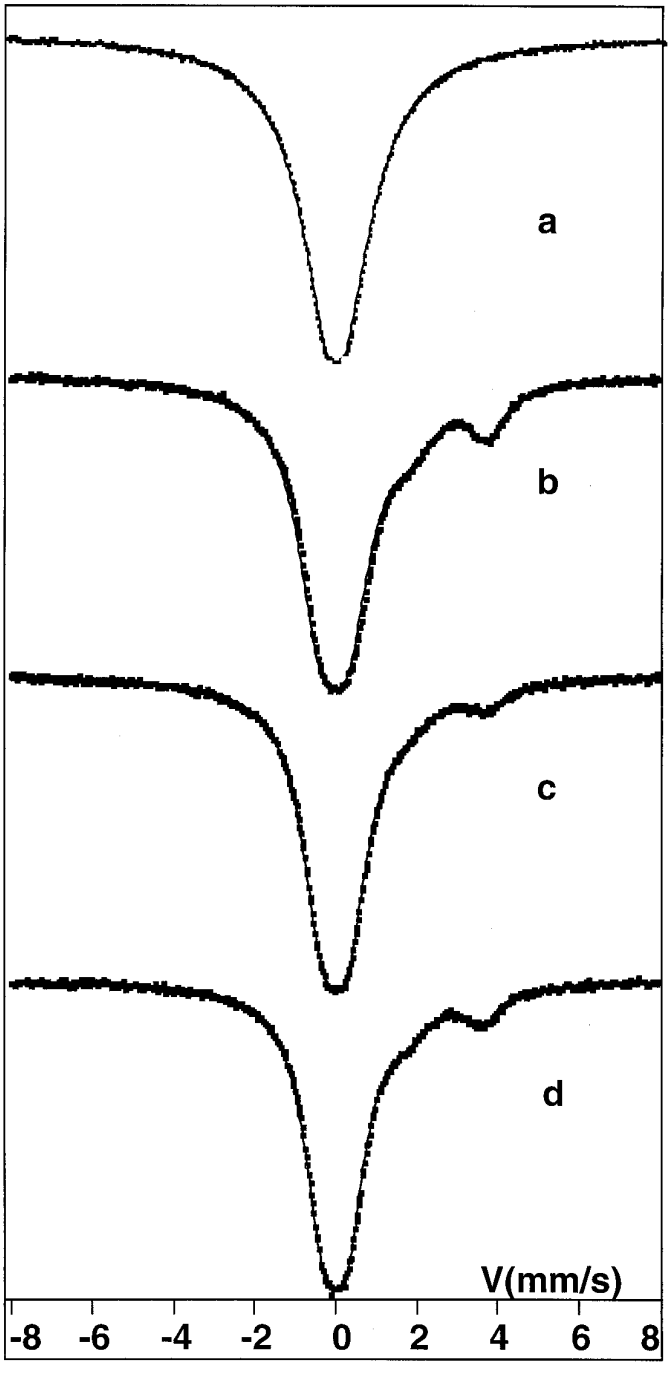

FIG. 1. Room temperature ^{119}Sn Mössbauer spectra of SnO_2 before and after grinding. (a) Pure SnO_2. (b) SnO_2 milled for 4 h with untreated steel tools. (c) SnO_2 milled for 4 h with hardened steel tools. (d) SnO_2 + Fe (3 wt%) milled for 4 h with hardened steel tools.

in the ground powder seems therefore to play an important role on the degree of reduction of the oxide. To confirm the latter assumption, we have performed a grinding experiment with a powder mixture of SnO_2 and 3 wt% of α-Fe with hardened steel tools. The latter iron amount has been evaluated from a grinding experiment performed in untreated steel media. Figure 1d indeed proves that a more marked reduction of SnO_2 takes place for the mixture containing iron than for the iron free powder (Fig. 1c). Moreover, the degree of reduction, $SnO_{1.74\pm0.03}$, is found to be similar to the result obtained from the first experiment (Fig. 1b). We finally mention that powders of tetragonal SnO decompose into metallic β-Sn and SnO_2 during grinding.

(*2*) *TiO_2–SnO_2*

Grinding experiments have been performed with both the rutile and anatase forms of TiO_2. Anatase is known to transform after 3 h of grinding with steel tools into the rutile form via TiO_2-II (a high pressure and high temperature form of TiO_2 with a α-PbO_2 type structure) (5). Figure 2 shows the XRD patterns of TiO_2–SnO_2 equimolar mixtures after increasing grinding times and as functions of the nature of grinding media. When milling is performed for 8 h either with the anatase form or with the rutile form, the XRD patterns (Figs. 2b, 2c, 2f, 2g) in either steel grinding media are almost identical. The diffraction peaks are broadened (due to crystallite size decrease and to lattice strain induced by grinding). In ground anatase–SnO_2 powders, the diffraction peak at $2\theta = 56°$ has disappeared, indicating that anatase TiO_2 has transformed or has formed solid solution. The more intense diffraction peaks of TiO_2 and SnO_2 are very close so that no diffraction peaks of anatase or other forms of TiO_2 have been indexed on XRD patterns. Only those of cassiterite SnO_2 have been indexed.

From these results, only the solubility of TiO_2 in SnO_2 can be calculated. The shift of SnO_2 diffraction peaks demonstrates that solid solution forms. Indeed, the unit cell volume after 8 h of grinding is of the same order for all experiments and is close to 71 $\pm$ 0.05 $Å^3$ in comparison with the unit cell volume of SnO_2 before grinding: 71.44 $Å^3$. In the TiO_2–SnO_2 system, although some authors assume that the lattice parameters follow Vegard's law (25, 49), Park *et al.* (26) report a positive deviation from that law. According to these authors, both the magnitude and the sign of the deviation can be predicted using a theory based on nonlinear second-order elasticity which takes into account the difference in ionic radii between Ti and Sn. They give the lattice parameters of SnO_2 as of function of TiO_2 content. Both results are given in the present paper, but our experiments are interpreted using the results of the most recent phase diagram of TiO_2–SnO_2 from Park *et al.* (26). According to the data of Park *et al.* (26), a composition of (mol%) $TiO_2 \approx 7 \pm 0.6$ in SnO_2 is reached. The solubility calculated from Vegard's law is $\approx 5 \pm 0.6$ mol%. Two hours of grinding are sufficient to achieve this solid solubility with the rutile form whereas longer times related to phase transformations are needed with the anatase modification.

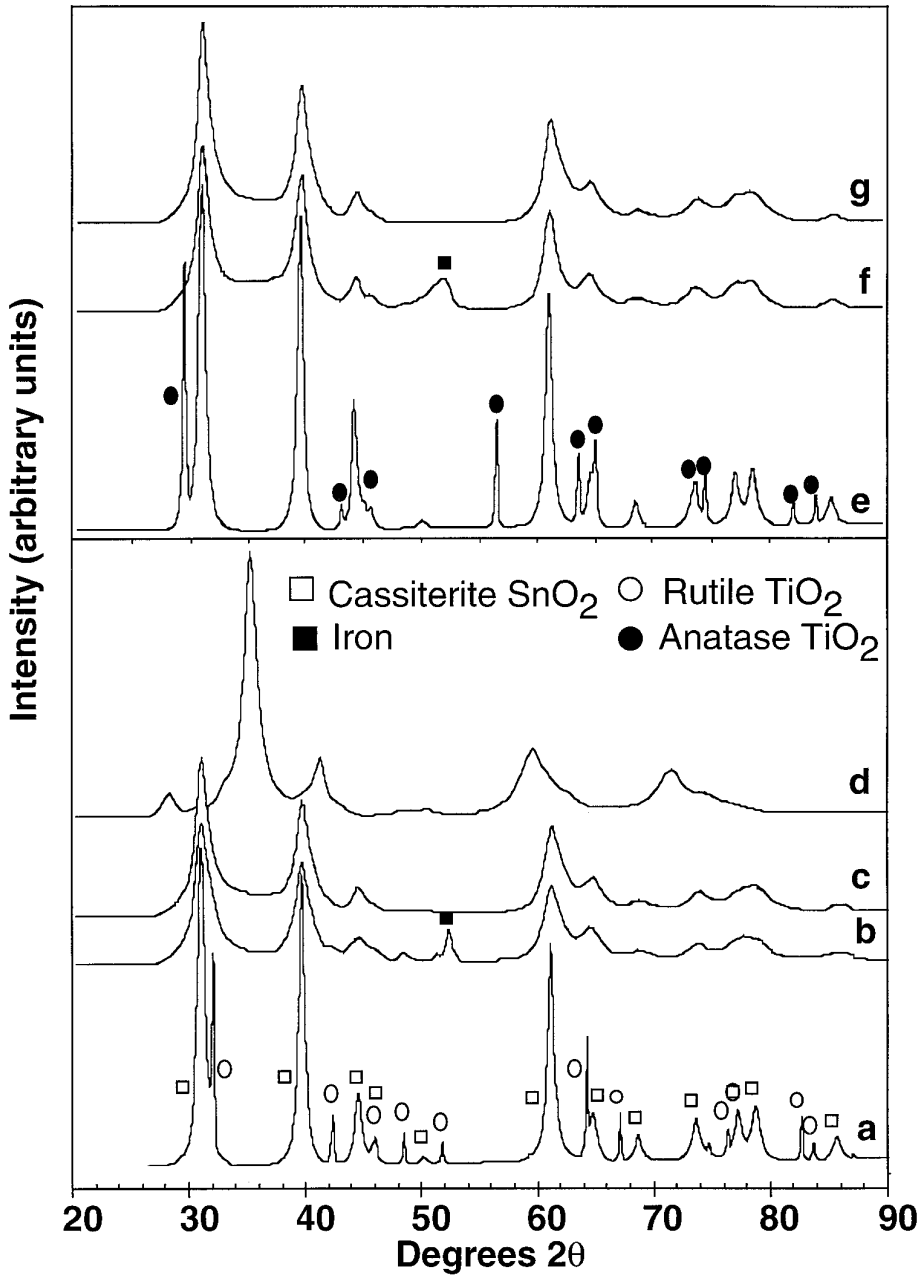

FIG. 2. X-ray diffraction patterns of TiO_2 and cassiterite SnO_2 powder mixtures. (a) Rutile TiO_2 and cassiterite SnO_2 initial powder mixtures, (b) milled for 8 h with untreated steel tools, (c) milled for 8 h with hardened steel tools, (d) milled for 8 h with stabilized zirconia tools: XRD pattern of stabilized zirconia. (e) Anatase TiO_2 and cassiterite SnO_2 initial powder mixtures, (f) milled for 8 h with untreated steel tools, (g) milled for 8 h with hardened steel tools.

The phase diagram TiO_2–SnO_2 is available only above 900°C and on the most recent phase diagram by Park *et al.* (26); at this temperature the maximum solubility of TiO_2 in SnO_2 is around 10% after annealing for a few days.

After grinding with steel tools the balls are covered with a bright layer which is rich in tin. In powders ground in untreated steel grinding media, ^{119}Sn Mössbauer spectroscopy shows the existence of reduced tin in the form of Sn^{2+} (Fig. 3a), which corresponds to the formation of a $SnO_{1.51\pm0.03}$ compound (Section 1, (6)). To avoid the reduction phenomenon of SnO_2 by steel grinding tools, which could influence the solid solubility, grinding has been performed in zirconia media. With a powder to ball weight ratio of 1/10, the energy transferred to the powder is not

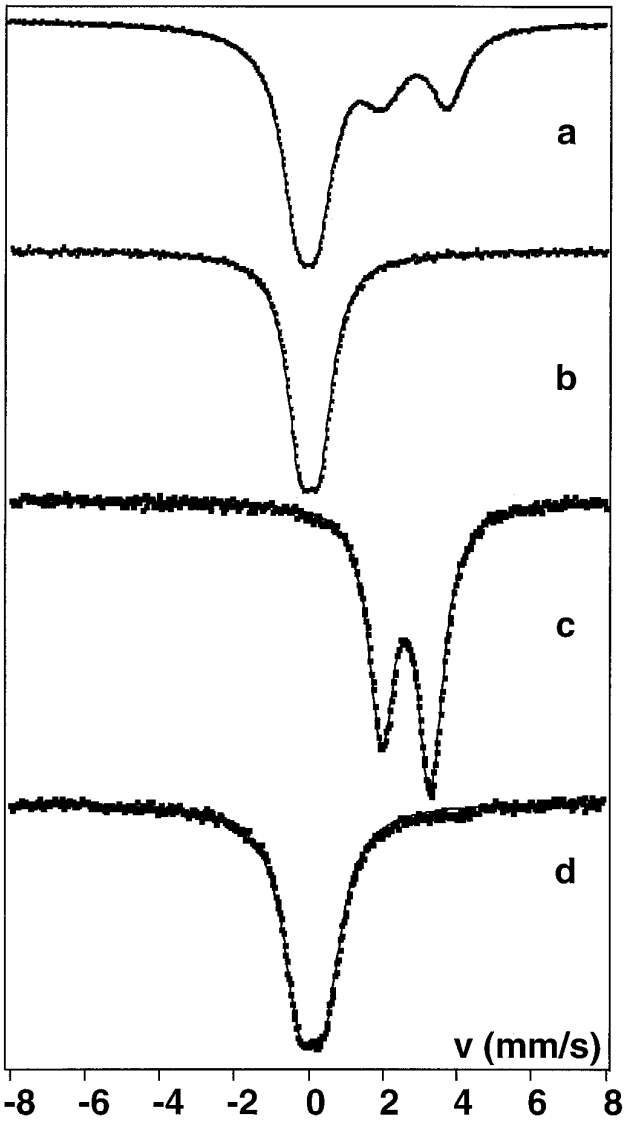

FIG. 3. Room temperature ^{119}Sn Mössbauer spectra of ground-based SnO_2 and SnO powder mixtures. (a) SnO_2–TiO_2 powder mixtures ground for 8 h with untreated steel tools. (b) SnO_2–V_2O_5 powder mixtures ground for 8 h with untreated steel tools. (c) Pure SnO. (d) SnO–V_2O_5 powder mixtures ground for 8 h with hardened steel tools.

sufficient to yield a significant solid solution. The powder to ball weight ratio has been increased, but the long grinding times necessary to form the solid solution meant that the contamination was too important to further analyze the results (Fig. 2d).

In conclusion, the solubility of TiO_2 in SnO_2 achieved by milling under our experimental conditions with steel tools remains far below the full solubility attainable under equilibrium conditions at 1430°C and above. It is on the order of the solubility reached under equilibrium conditions slightly below 900°C.

(*3*) *SnO_2–V_2O_5*

(*3.a*) *Ground powders.* The development of phases in SnO_2–V_2O_5 ground powders has been followed by X-ray diffraction and the behavior depends upon the grinding media used, as can be seen in Fig. 4. When milling is performed with zirconia or hardened steel (Fig. 4b), the intensities of the V_2O_5 diffraction peaks decrease strongly at the beginning of grinding and then stabilize, while with untreated steel media (Fig. 4a), the V_2O_5 diffraction peaks have completely disappeared after 4 h.

The powders have been milled for long times in each milling media and no important contamination by steel or zirconia is visible on XRD patterns. With untreated steel tools, the characteristic diffraction peak of alpha iron at $2\theta \approx 52.4°$ is not present on XRD patterns except after 10 h of milling. Nevertheless, between 6 and 8 h, transient phases form which can be identified either as Fe–V–O compounds or as vanadium oxides of a lower degree of oxidation. These observations prove again that milling media may interact with oxides. This is confirmed by ^{57}Fe Mössbauer spectroscopy, since the spectrum displays a doublet related to a Fe^{3+} component. With hardened steel tools, the absence of a significant resonant signal on ^{57}Fe Mössbauer spectra demonstrates that there is at most a weak contamination by steel. No reduction of SnO_2 in all ground powders is observed by ^{119}Sn Mössbauer spectroscopy. This is an important result considering that SnO_2 milled with untreated grinding tools either alone (Fig. 1, (6)) or with TiO_2 is partly reduced (Fig. 3). In the same way, the contamination of powders by zirconia is surprisingly not significant.

(*3.b*) *Powders after DSC experiments.* DSC curves of ground powders are presented in Fig. 5 for different milling times and grinding tools. They display three endothermic peaks around 625 ± 7°C, 650 ± 10°C, and 708 ± 3°C in the case of powders milled in untreated steel media. Those milled in either zirconia or hardened steel media display two endothermic peaks in the range 640 ± 10°C and around 670 ± 5°C (Table 1). The DSC experiment on the initial powder exhibits only an endothermic peak at 677°C corresponding to the melting point of V_2O_5. The peak around 670°C (zirconia or hardened steel tools, Fig. 5b) is attributed to the melting of V_2O_5 and, according to the results of other authors (23, 37, 50), that around 650°C (untreated steel tools, Fig. 5a) corresponds to the melting of a slightly reduced disordered V_2O_5. Indeed it has often been reported during the preparation of V_2O_5-based catalysts that some V_2O_5 is reduced even though no reduced phase could be detected by X-ray analysis (23, 31, 33, 37).

The V_2O_5 solubility in SnO_2 increases after DSC experiments at 800°C. The peak located around ≈625°C for powders ground with untreated steel media and around 640°C for powders ground in other media should correspond to

solid solution formation or, considering the aforementioned remarks, to the formation of a reduced vanadium oxide with V^{4+} ions. The latter peak is not observed on the DSC curve of initial powder mixtures. Indeed, V_2O_5

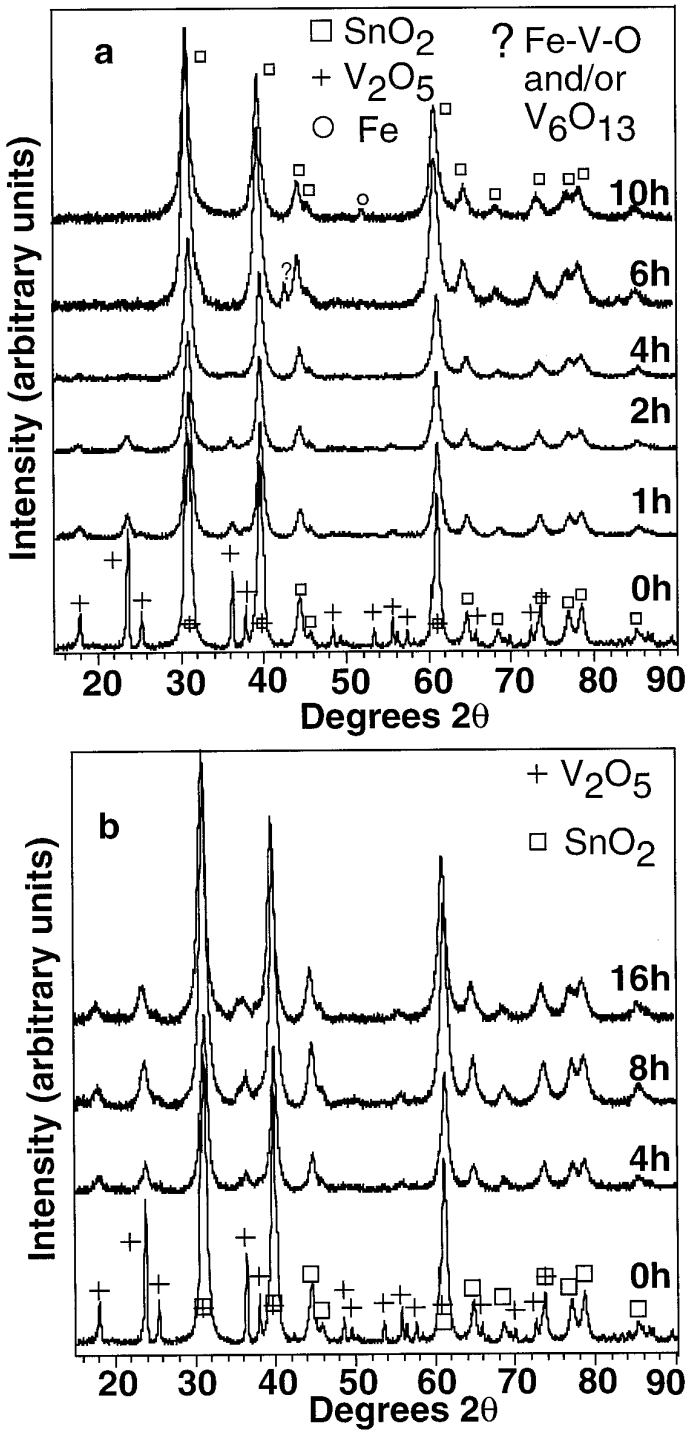

FIG. 4. X-ray diffraction patterns of SnO_2–V_2O_5 powder mixtures milled (a) with untreated steel tools and (b) with stabilized zirconia tools.

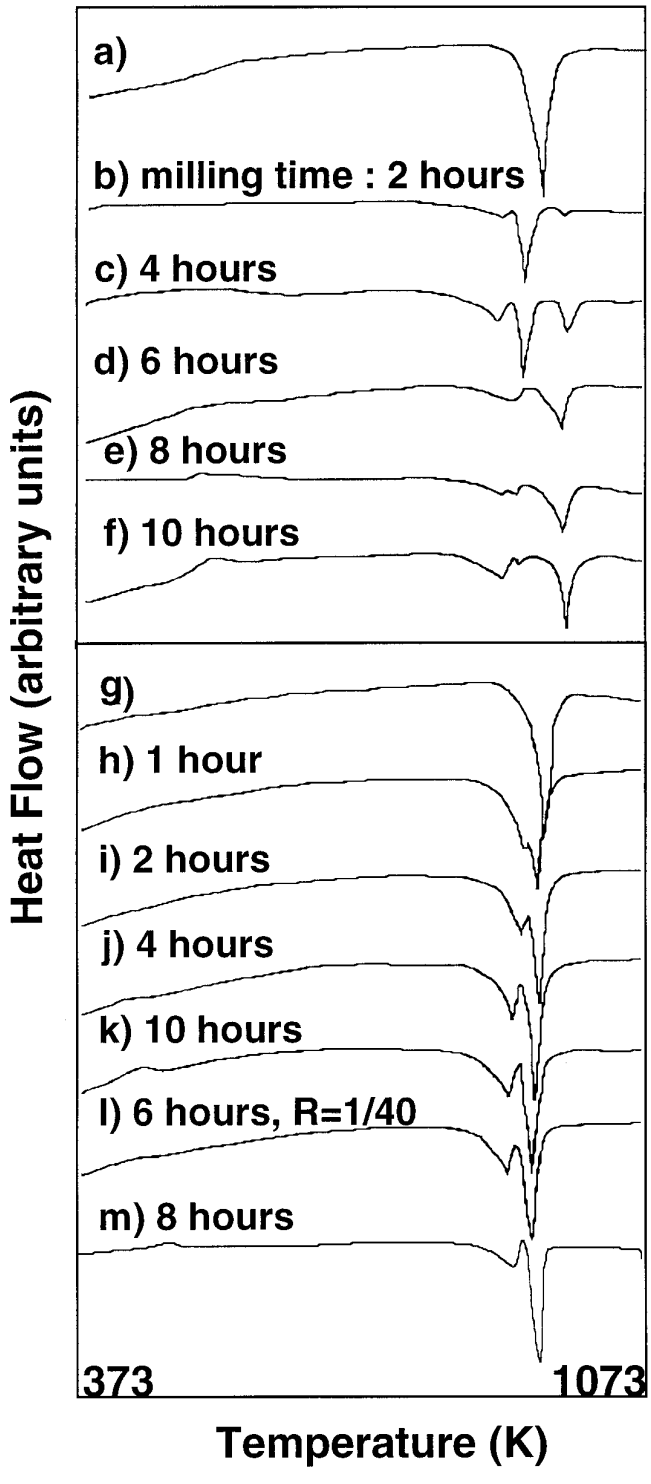

FIG. 5. DSC curves of SnO_2–V_2O_5 powder mixtures. (a–g) Starting SnO_2–V_2O_5 powder mixtures, (b–f) ground in untreated steel media. (h–l) SnO_2 + V_2O_5 ground in stabilized zirconia media. (m) SnO_2 + V_2O_5 ground in hardened steel media.

TABLE 1
Endothermic Peaks on DSC Curves of Milled SnO_2–V_2O_5 Powders

Milling media	Reduction of V_2O_5 or solid solution formation	V_2O_5 melting	V_6O_{13} melting
Untreated steel	625 ± 7°C	650 ± 10°C	708 ± 3°C
Hardened steel	640 ± 10°C	670 ± 5°C	
Stabilized zirconia	640 ± 10°C	670 ± 5°C	
Pure V_2O_5		677°C	
Fe (3 wt%) + SnO_2 + V_2O_5 hardened steel media		670 ± 5°C	710 ± 3°C

decomposes by losing oxygen at $T > 680$°C (51, 52) and thus solution forms during the melting of V_2O_5. Moreover, grinding is known to mechanically activate reactions, which may explain the shift of this peak to lower temperatures (≈625°C) for ground powders.

The other endothermic peak around 710°C can be attributed to the melting of V_6O_{13} which occurs at 710°C (36, 53–55). The presence of V_6O_{13} in synthesized SnO_2–V_2O_5 composites has often been observed (21, 23, 37).

XRD patterns of powders ground with untreated steel tools after DSC experiments are represented in Fig. 6: they exhibit the characteristic diffraction peaks of SnO_2 and V_2O_5 and also new diffraction peaks. The latter diffraction peaks are indexed as V_6O_{13} but they may as well be attributed to a Fe–V–O compound. According to the JCPDS files, the main peaks of the XRD pattern of a $Fe_{0.13}V_{0.87}O_{2.17}$ compound are located at the same positions as those of V_6O_{13} (56). This formation of a Fe–V–O compound is further confirmed by Mössbauer spectroscopy which shows the presence of an iron(3+)–vanadium compound before and after DSC experiments and also by X-ray diffraction: some diffraction peaks of V_6O_{13} are too strong compared with the relative intensities expected from the JCPDS file. Finally a compound like $Fe_{0.13}V_{0.87}O_{2.17}$ may in fact be considered as V_6O_{13} with Fe in substitutional site (V_6O_{13} : $V_3^{5+}V_2^{4+}V^{3+}O_{13}^{2-}$). In both of the other grinding media, the XRD patterns are identical before and after DSC experiments except for sharper diffraction peaks after heating.

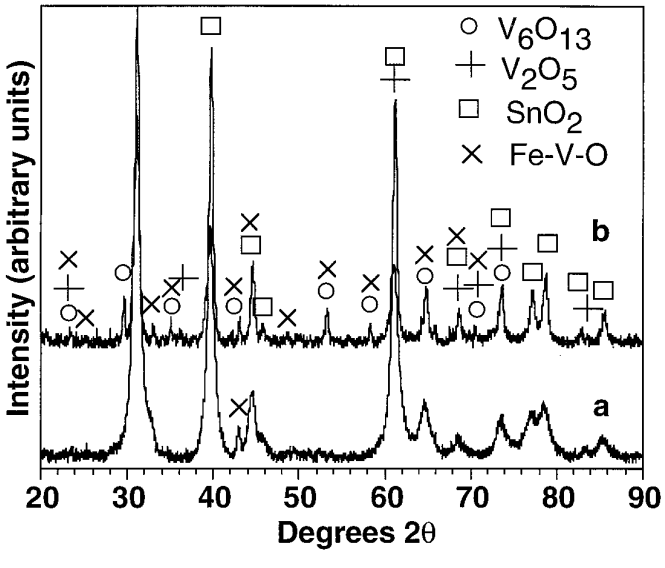

FIG. 6. X-ray diffraction patterns of SnO_2–V_2O_5 powder mixtures milled for 6 h in untreated steel media (a) and after DSC experiment (b).

(*3.c*) *Solubility characterization.* The diffraction peaks of SnO_2 before and after DSC experiments are more or less shifted according to the nature of grinding media. Such a shift cannot result from contamination by grinding tools. That is excluded from ^{119}Sn Mössbauer spectroscopy and from grinding experiments of SnO_2 alone, which means that solid solutions form. The variation of the unit cell volumes with grinding times before and after DSC experiments with both steel and zirconia tools are presented in Fig. 7. The unit cell volume decrease is stronger for powders ground with untreated steel tools than for powders ground with hardened steel or zirconia tools. A maximum solubility close to 1.8 ± 0.05 wt% V_2O_5 (3.1 at.% V^{4+} in SnO_2) is achieved when untreated steel media are used for grinding. The solubility reached with zirconia and hardened steel tools is not significant enough to be considered. By contrast, the solubility attained after DSC experiments has strongly increased in all cases: without grinding ≈1.9 ± 0.05 wt% (3.3 at.% V^{4+} in SnO_2), after grinding in both steel media (R = 1/40) ≈3.2 ± 0.05 wt% V_2O_5 (5.5 at.% V^{4+} in SnO_2), and after grinding with zirconia tools (R = 1/10) ≈2.2 ± 0.05 wt% (3.8 at.% V^{4+} in SnO_2). It can also be observed that the larger solubilities are reached after DSC experiments on powders ground for short times (Fig. 7). As mentioned above grinding mechanically activates reactions. Long grinding times favor oxygen losses during subsequent heat treatments. Strongly reduced vanadium oxides form which limit the solid solution formation reaction.

The resulting solubility values are difficult to compare with the data of other authors because results are widely scattered and calculation methods are often different (22–23, 29). It seems more appropriate to compare our results with those of Fujiyoshi *et al.* (23) ≈0.9 wt% because the solubility has been calculated in the same way. Grinding experiments with untreated steel tools give rise to slightly larger solubilities. The possibility of formation of a Fe–Sn–O oxide or of a Fe–Sn intermetallic compound can be

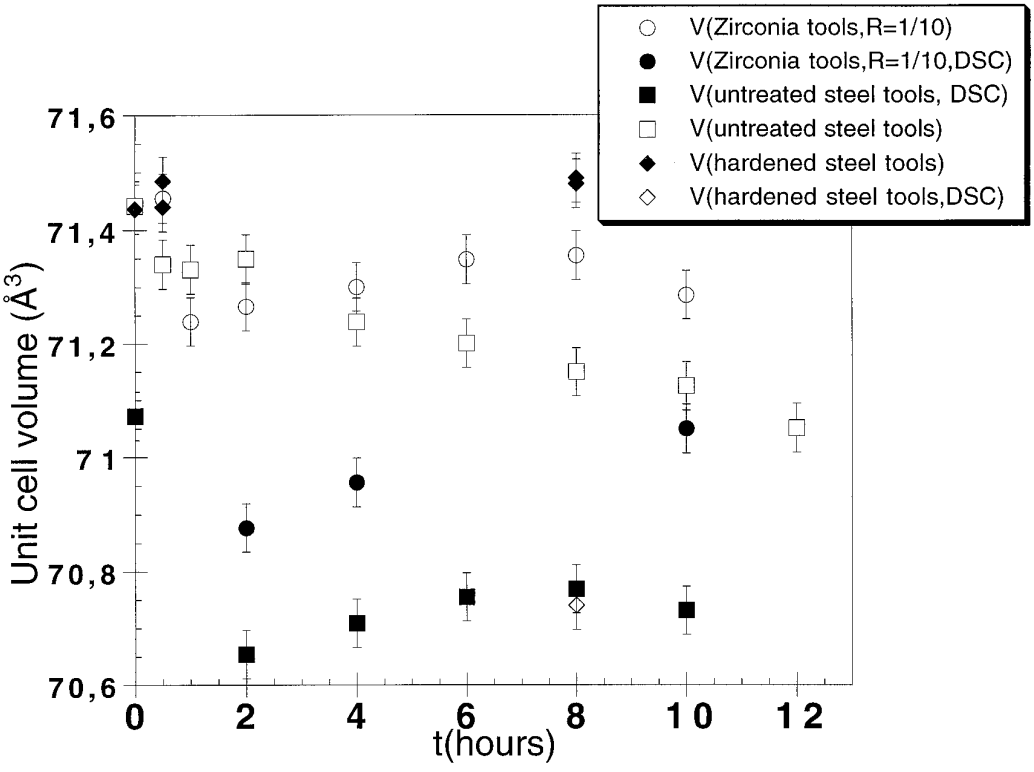

FIG. 7. Unit cell volume of SnO_2 before and after DSC experiments as a function of grinding time and of the nature of grinding tools.

discarded since ^{119}Sn Mössbauer spectra only show a SnO_2 line (Fig. 3b). On the other hand, grinding experiments followed by heat treatments allow obtaining a significant solubility increase.

(*3.d*) *Discussion.* The different experimental results found when grinding is performed either with untreated steel tools or with treated steel or zirconia must be attributed to the fact that oxidation–reduction reactions take place between tools and oxide powders significantly only in the former case. As shown in Section 1, the degree of reduction of tin oxide is related to the amount of Fe which is incorporated into the powders during grinding. The sole presence of reduced vanadium oxides seems not sufficient to form solid solution. We have therefore to conclude that it is the combined action of Fe and of SnO_2 which is responsible for the increase of the solid solubility which is observed when SnO_2–V_2O_5 powders are ground with untreated steel tools. In our SnO_2–V_2O_5 grinding experiments, no reduction of SnO_2 is noticed, while we have shown (Section 1, (6)) that SnO_2 is more or less reduced when ground with steel tools. That shows that SnO_x might have been reoxidized by another compound, which can only be V_2O_5 (only Fe^{3+} is observed in the powders).

Experiments were performed with SnO instead of SnO_2 to confirm the assumption that the vanadium solubility in SnO_2 depends on the degree of reduction of SnO_2. The ^{119}Sn Mössbauer spectrum of ground powders (Fig. 3d) displays a broad peak corresponding to SnO_2 and the melting of either disordered V_2O_5 or V_6O_{13} is not observed on DSC curves (Section 1). The XRD pattern of ground SnO–V_2O_5 powders with very broad peaks doesn't allow precise calculation of the solubility, although a solubility of $\approx 55 \pm 7$ at.% V^{4+} (25 wt% V_2O_5) is deduced from a rough calculation of the SnO_2 unit cell volume. After DSC experiments, a solubility of $\approx$3.0 wt% (5.1 at.% V^{4+}) is reached, in agreement with the value obtained after grinding and DSC experiments. This tends to prove that it represents the solubility limit.

These results are of interest in the following perspective: V_2O_5–SnO_2 and V_2O_5–TiO_2 composite powders are widely studied as selective oxidation catalysts for hydrocarbons (21–23). The high activity of the SnO_2/V_2O_5 catalyst is thought to originate from the easy removal of oxygen from the structure of supported V_2O_5 (21–22, 32, 38). In a general way, V_2O_5 at the surface, in contact with SnO_2 (or TiO_2) grains, tends to reduce and solid solution forms. The reason V_2O_5 releases oxygen when it is in contact with MO_2, while it does not if it is not in contact with such oxides, has remained rather speculative so far.

Three main types of interpretations (33, 38, 57) have

been put forward (mainly for TiO_2–V_2O_5 catalysts) to explain the influence of the support on the structure of V_2O_5. Such a support:

(i) induces a preferential exposure of V=O double bonds (32);
(ii) modifies the strength of V=O double bonds (21, 22, 35, 39);
(iii) induces an unusual vanadium oxide surface structure with reduced or quasi-amorphous phases of V_2O_5 at the surface of the support (21, 23, 33). Further assumptions have also been put forward, some of which may be useful in the present context. Some authors suggest either that during heat-treatment V^V ions react with specific sites of the TiO_2 anatase surface, or even that the interaction of V_2O_5 with the TiO_2 surface stabilizes the valence four state of vanadium. It is also assumed that the oxygen loss of V_2O_5 is related to the presence of hydroxyl groups at the surfaces of SnO_2 or TiO_2 grains (31–34, 37, 57).

Our grinding experiments show that it is the reoxidation of tin oxide which explains the presence of reduced vanadium oxides at the surface of tin oxide grains.

(*4*) *TiO_2–V_2O_5*

(*4.a*) *Experimental results.* Grinding experiments have been performed mainly with anatase titania because this modification is reported to be a more efficient support of V_2O_5-based catalysts than rutile (32, 33). Milling in untreated steel media induces a strong decrease in the intensity of V_2O_5 diffraction peaks, as can be seen in Fig. 8, and the formation of the rutile form. In hardened steel media, the diffraction peaks of V_2O_5 are always present but broaden and TiO_2-II is the major titania phase (Figs. 8a–8d). However, the solubility of V_2O_5 in TiO_2 cannot be estimated after milling with hardened steel tools as V^{4+} is supposed to form solid solution only with the rutile form. In untreated steel media, it is difficult to calculate the lattice parameters from XRD patterns from such broad diffraction peaks. We estimate, nevertheless, according to Vegard's law, a solubility value close to 43 at.% V^{4+}.

When grinding is performed with the rutile modification in untreated steel media (Figs. 8e–8g), rutile is the major phase after 8 h of grinding while the intensities of V_2O_5 diffraction peaks have strongly decreased. Moreover, with hardened steel or zirconia tools, V_2O_5 does not disappear and remains the major phase. The calculated solid solubility is ≈40 ± 1 at.% with untreated steel tools and 8.2 ± 0.6 .at% with hardened steel grinding tools.

DSC experiments on these ground powders display a broad endothermic peak close to 680°C usually ascribed to V_2O_5 melting. However, during the preparation of anatase TiO_2–V_2O_5 catalysts, the anatase–rutile transition is reported to be accompanied simultaneously by the formation

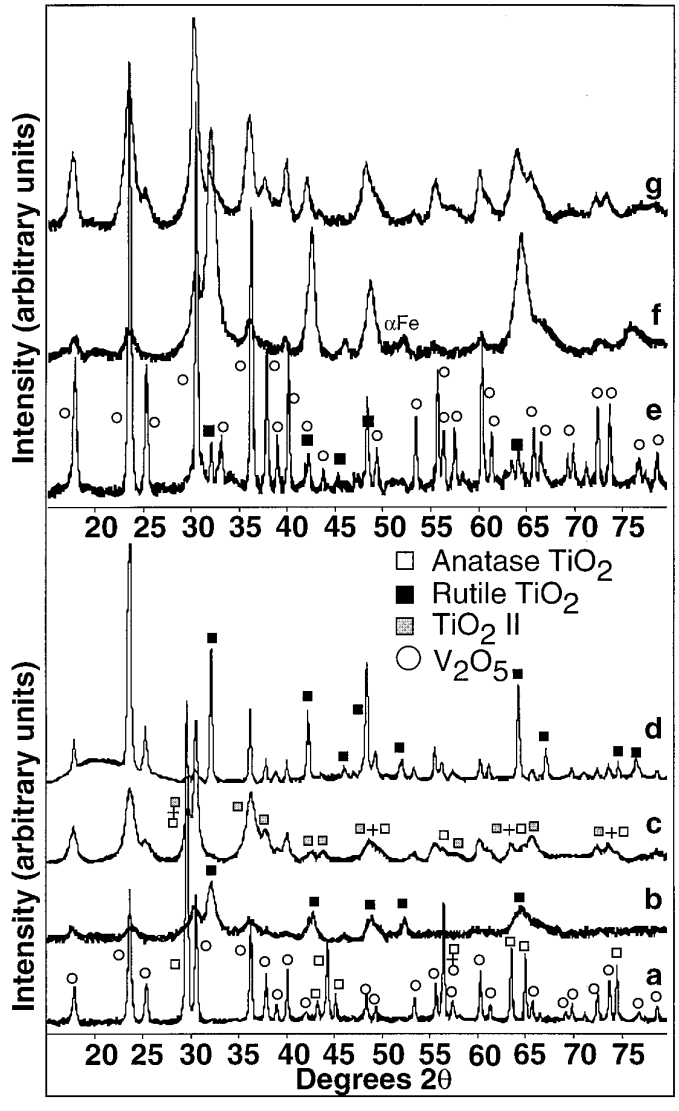

FIG. 8. X-ray diffraction patterns of milled TiO_2 and V_2O_5 powder mixtures. (a) Anatase TiO_2 and V_2O_5 initial powder mixtures. (b) Anatase TiO_2 and V_2O_5 milled for 8 h with untreated steel tools. Identified phases: rutile TiO_2 and V_2O_5. (c) Anatase TiO_2 and V_2O_5 milled for 4 h with hardened steel tools. Identified phases: anatase TiO_2, TiO_2 II, and V_2O_5. (d) Anatase TiO_2 and V_2O_5 milled for 4 h with hardened steel tools and after DSC experiments. Identified phases: rutile TiO_2 and V_2O_5. (e) Rutile TiO_2 and V_2O_5 initial powder mixtures. (f) Rutile TiO_2 and V_2O_5 milled for 8 h with untreated steel tools. Identified phases: rutile TiO_2 and V_2O_5. (g) Rutile TiO_2 and V_2O_5 milled for 8 h with hardened steel tools. Identified phases: rutile TiO_2 and V_2O_5.

of the solid solution of V^{4+} in rutile TiO_2 and to occur at ≈700°C (31, 39). This could explain the presence of only one peak on the DSC curves. XRD patterns of DSC samples exhibit the diffraction peaks of V_2O_5 and rutile TiO_2. Whatever the starting titania phase, for powders ground with no contaminating tools and after DSC experiment, a solubility of ≈19 at.% V^{4+} is calculated, which is much

greater than usually published values (≈8 wt% V_2O_5 ≈7.6 at.% V^{4+}).

(*4.b*) *Discussion.* These results confirm the aforementioned hypothesis that the presence of reduced MO_2 induces reduction of V_2O_5 and solid solution formation. TiO_2 is known to be easily nonstoichiometric with Ti^{3+} ions. The latter tendancy is expected to be emphasized by grinding in reducing media as oxygen deficiency in rutile TiO_{2-x} is accommodated by crystallographic shears (59). Lopska *et al.* (30) have observed that the concentration of Ti^{3+}, after preparation of a TiO_2–V_2O_5 catalyst by annealing, strongly decreases when TiO_2 is in the presence of V_2O_5 and that reduced vanadium oxides form. Centi *et al.* (33) also offer this hypothesis that during heat treatment of TiO_2–V_2O_5 catalysts, there is dehydroxylation of OH surface sites with formation of Ti^{3+} sites and oxygen vacancies. The presence of oxygen vacancies due to the presence of tin or titanium atoms in lower oxidation states is expected to induce the reduction of V_2O_5 at the interface between V_2O_5 and MO_2 (33). During grinding experiments with contaminating tools or during preparation of catalysts by heat treatments, MO_2 is submitted to reduction phenomena and is oxidized again by oxygen from V_2O_5. Due to its chemical nature and to its lamellar structure, V_2O_5 may easily lose oxygen under such reducing conditions.

During grinding experiments, the interaction of V_2O_5 with MO_2 is strengthened in different ways. It contributes first to introduce defects which destabilize the V_2O_5 structure. Second grinding induces a strong decrease in crystallite size and V_2O_5 is reported to decompose faster as ultrafine grains than as classical powder (37, 39, 58). Finally, as all reactants are brought into intimate contact by grinding, V_2O_5 easily loses oxygen. This latter effect is amplified during heat treatment.

CONCLUSION

Grinding experiments followed by heat treatments enable substantial solid solubilities in binary oxide mixtures. The solubility after grinding only depends strongly on the nature of grinding media in V_2O_5 based systems. These results demonstrate again that the nature of grinding media may play an important role, mainly either by contaminating or by interacting with the ground powders. For the SnO_2–TiO_2 system, grinding in both steel media leads to the formation of a solid solution with ≈5 ± 0.6 mol% TiO_2 in SnO_2 according to Vegard's law. In V_2O_5-based systems, grinding in untreated steel media yields increased solid solubilities in comparison with published values: ≈1.7 and ≈20 wt% of V_2O_5 in SnO_2 and TiO_2, respectively. With hardened steel tools, the solubility of V_2O_5 in SnO_2 is negligible and that in TiO_2 is ≈4 wt%.

The experiments in V_2O_5-based systems have demonstrated that the interaction between SnO_2 or TiO_2 and V_2O_5 results from the fact that during grinding SnO_2 and TiO_2 are slightly reduced and are brought into intimate contact with V_2O_5. Thus under such conditions, V_2O_5 itself is reduced and solid solutions form. The latter reduction reactions are not predicted from the relative affinities of Sn, Ti, and V for oxygen. However such reactions may be induced under the conditions prevailing during milling. Such conclusions would moreover be consistent with the observations that V_2O_5 released its oxygen in catalysts when it is supported on MO_2 (M = Ti, Sn) oxides (Section 3d).

The final product exhibits a homogeneous mixture of both oxides at the nanometric scale with slightly reduced rather amorphous V_2O_5 layers at the surface of reoxidized SnO_2 or TiO_2 grains. The high chemical activity of the MO_2/V_2O_5 catalyst originates from the easy removal of oxygen from the structure of supported V_2O_5, more precisely from the interfaces between both oxides (32, 38) when the vanadia is present in the form of highly disordered, amorphous or reduced species (21, 22, 32, 33, 37, 38). Thus the binary mixtures synthesized by grinding, which induce the formation of a large density of interfaces, as well as some V_2O_5 reduction, could be of interest in the catalysis field if a sufficiently large specific area could be reached.

REFERENCES

1. J. J. De Barbadillo, *Key Eng. Mater.* **77–78,** 187 (1993).
2. E. Gaffet, M. Abdellaoui, and N. Malhouroux-Gaffet, *Mater. Trans. JIM* **36,** 198 (1995).
3. P. Matteazzi and G. Le Caër, *J. Am. Ceram. Soc.* **74,** 1382 (1991).
4. C. C. Koch, *Nanostructured Mater.* **2,** 109 (1993).
5. S. Begin-Colin, G. Le Caër, A. Mocellin, and M. Zandona, *Phil. Mag. Lett.* **69,** 1 (1994).
6. S. Begin-Colin, G. Le Caër, M. Zandona, E. Bouzy, and B. Malaman, *J. Alloys Compounds* **227,** 157 (1995).
7. I. S. Polkin, E. Kaputkin, and A. B. Borzov, *in* "Structural Applications of Mechanical Alloying," (F. H. Froes and J. J. de Barbadillo, Eds.), p. 251. ASM International, Materials Park, Ohio, 1990.
8. E. Gaffet, F. Faudot, and M. Harmelin, *J. Alloys Compounds* **194,** 23 (1993).
9. E. Gaffet, C. Louison, M. Harmelin, and F. Faudot, *Mater. Sci. Eng. A* **134,** 1380 (1991).
10. F. Faudot, E. Gaffet, and M. Harmelin, *J. Mater. Sci.* **28,** 2669 (1993).
11. R. Sundaresan and F. H. Froes, *in* "New Materials by Mechanical Alloying Techniques" (E. Arzt and L. Schultz, Eds.), p. 253. DGM Informationsgesellshaft, Oberursel, 1989.
12. Renato De Araujo Pontès, Thèse INPL, Nancy, 1992.
13. G. Le Caër, R. De Araujo Pontès, D. Osso, S. Bégin-Colin, and P. Matteazzi, *J. Phys.* **4,** C3–233 (1994).
14. I. J. Lin, S. Nadiv, and P. Bar-On, *Thermochim. Acta* **148,** 301 (1989).
15. P. A. Zielinski, R. Schulz, S. Kaliaguine, and A. Van Neste, *J. Mater. Res.* **8,** 2985 (1993).
16. T. Ikeya and M. Senna, *J. Mater. Sci.* **22,** 2497 (1987).
17. T. Ikeya and M. Senna, *J. Non-Crystallogr. Solids* **105,** 243 (1988).
18. D. Michel, F. Faudot, E. Gaffet, and L. Mazerolles, Revue de Métallurgie, 219 (février 1993).
19. F. Wolf, G. LeCaër, S. Begin-Colin, and G. Braichotte, "Proceedings

of the First International Conference on Mechanochemistry, Kosice, 23–26 March 1993.'' Interscience, Cambridge.
20. F. Wolf, Thèse de l'INPL, Nancy, 1995.
21. A. Anderson, *J. Catal.* **69,** 465 (1981).
22. W. M. H. Sachtler, G. J. H. Dorgelo, J. Fahrenfort, and R. J. H. Voorhoeve, *Recueil* **89,** 461 (1970).
23. K. Fujiyoshi, H. Yokoyama, F. Ren, and S. Ishida, *J. Am. Ceram. Soc.* **76,** 981 (1993).
24. N. N. Padurov, *Naturwissenschaften* **43,** 395 (1956).
25. D. Garcia and D. Speidel, *J. Am. Ceram. Soc.* **55,** 322 (1972).
26. M. Park, T. E. Mitchell, and A. H. Heuer, *J. Am. Ceram. Soc.* **58,** 43 (1975).
27. S. Ishida, F. Fujimura, K. Fujiyoshi, and S. Kanaoka, *Yogyo Kyokaishi* **91,** 546 (1983).
28. S. Ishida, F. Ren, and N. Takeuchi, *J. Am. Ceram. Soc.* **76,** 2644 (1993).
29. T. Takahashi, S. Kodaira, T. Matsushita, I. Yamai, and H. Saito, *Yogyo Kyokaishi* **83,** 33 (1975).
30. P. Lostak, Z. Cernosek, E. Cernoskova, L. Benes, J. Kroutil, and V. Rambousek, *J. Mater. Sci.* **28,** 1189 (1993).
31. M. A. Tena, G. Monros, J. Carda, E. Cordoncillo, and P. Escribano, *British Ceram. Trans.* **94,** 10 (1995).
32. A. Vejus and P. Courtine, *J. Solid State Chem.* **23,** 93 (1978).
33. G. Centi, E. Giamello, D. Pinelli, and F. Trifiro, *J. Catal.* **130,** 220 and 238 (1991).
34. E. Gillis and E. Boesman, *Phys. Stat. Sol.* **14,** 337 (1966).
35. A. Anderson and S. T. Lundin, *J. Catal.* **58,** 383 (1979); *J. Catal.* **65,** 9 (1980).
36. A. Anderson, *Acta Chem. Scand.* **10,** 623 (1956).
37. Lars S. T. Anderson, *J. Chem. Soc. Faraday Trans. B* **75,** 1356 (1978).
38. P. F. Miquel, C. H. Hung, and J. L. Katz, *J. Mater. Res.* **8,** 2404 (1993).
39. F. Roozeboom, M. C. Mittelmeijer-Harzelege, J. A. Mouljin, J. Medema, V. H. J. De Beer, and P. J. Gilling, *J. Phys. Chem.* **84,** 2783 (1980).
40. V. V. Boldyrev, *J. Chim. Phys.* **83,** 821 (1986).
41. L. Takacs, *Mater. Lett.* **13,** 119 (1992).
42. L. Takacs, *Nanostruct. Mater.* **2,** 241 (1993).
43. P. Matteazzi and G. Le Caër, *Mater. Sci. Eng. A* **149,** 135 (1991).
44. P. Matteazzi and G. Le Caër, *J. Am. Ceram. Soc.* **75,** 2749 (1992).
45. G. B. Schaffer and P. G. McCormick, *Scripta Metall.* **23,** 835 (1989).
46. G. B. Schaffer and P. G. McCormick, *Metall. Trans. A* **21,** 2789 (1990).
47. M. Abdellaoui and E. Gaffet, *Acta Metall. Mater.* **43,** 1087 (1995).
48. M. Abdellaoui and E. Gaffet, *J. Alloys Comp.* **209,** 351 (1994).
49. T. C. Yuan and A. V. Virkar, *J. Am. Ceram. Soc.* **71,** 12 (1988).
50. V. Satavav, *Collection Czechoslov. Chem. Commun.* **24,** 3297 (1959).
51. F. Maillot, Thèse de Docteur-Ingénieur, Lyon 1, 1975.
52. S. Desagher, L. Tsé Yu, and R. Buvet, *J. Chim. Phys.* **72,** 390 (1975).
53. G. V. Samsonov, ''The Oxide Handbook.'' IFI Plenum, New York, 1973.
54. F. Théobald, *Revue Roumaine de Chimie* **23,** 887 (1978).
55. F. Théobald, R. Cabala, and J. Bernard, *J. Solid State Chem.* **17,** 431 (1976).
56. K. Abraham *et al*., *J. Electrochem. Soc.* **128,** 2493 (1981).
57. G. Busca, G. Centi, L. Marchetti, and F. Trifiro, *Langmuir* **2,** 568 (1986).
58. R. J. D. Tillet and B. G. Hyde, *J. Phys. Chem. Solids,* **31,** 1613 (1970).
59. B. G. Hyde and S. Anderson, ''Inorganic Crystal Structures,'' p. 98. Wiley, New York, 1989.